ARMY RESEARCH LABORATORY

Quantitative Three-Dimensional Analysis of Structural Damage in Penetrated Magnesium via XCT

by William H. Green, Kyu C. Cho, Jonathan S. Montgomery, and Herbert Miller

ARL-TR-5359 **September 2010**

NOTICES

Disclaimers

The findings in this report are not to be construed as an official Department of the Army position unless so designated by other authorized documents.

Citation of manufacturer's or trade names does not constitute an official endorsement or approval of the use thereof.

Destroy this report when it is no longer needed. Do not return it to the originator.

Army Research Laboratory
Aberdeen Proving Ground, MD 21005-5069

ARL-TR-5359 **September 2010**

Quantitative Three-Dimensional Analysis of Structural Damage in Penetrated Magnesium via XCT

William H. Green, Kyu C. Cho, Jonathan S. Montgomery, and Herbert Miller
Weapons and Materials Research Directorate, ARL

REPORT DOCUMENTATION PAGE	Form Approved OMB No. 0704-0188

1. REPORT DATE *(DD-MM-YYYY)*	2. REPORT TYPE	3. DATES COVERED (From - To)
September 2010	Final	February 2009–March 2010

4. TITLE AND SUBTITLE
Quantitative Three-Dimensional Analysis of Structural Damage in Penetrated Magnesium via XCT

5a. CONTRACT NUMBER

5b. GRANT NUMBER

5c. PROGRAM ELEMENT NUMBER

6. AUTHOR(S)
William H. Green, Kyu C. Cho, Jonathan S. Montgomery, and Herbert Miller

5d. PROJECT NUMBER
W911NF-072-0073

5e. TASK NUMBER

5f. WORK UNIT NUMBER

7. PERFORMING ORGANIZATION NAME(S) AND ADDRESS(ES)
U.S. Army Research Laboratory
ATTN: RDRL-WMM-D
Aberdeen Proving Ground, MD 21005-5069

8. PERFORMING ORGANIZATION REPORT NUMBER
ARL-TR-5359

9. SPONSORING/MONITORING AGENCY NAME(S) AND ADDRESS(ES)

10. SPONSOR/MONITOR'S ACRONYM(S)

11. SPONSOR/MONITOR'S REPORT NUMBER(S)

12. DISTRIBUTION/AVAILABILITY STATEMENT
Approved for public release; distribution is unlimited.

13. SUPPLEMENTARY NOTES

14. ABSTRACT
X-ray computed tomography (XCT) has been shown to be an important non-destructive evaluation (NDE) technique for revealing the spatial distribution of ballistically-induced damage in metals, ceramics, and encapsulated ceramic structures. Previous and ongoing work in this area includes assessment of ballistically induced damage in relatively lightweight individual ceramic targets and ceramic armor panels. In this report, the ballistic damage in a novel Mg alloy sample was completely scanned and extensively evaluated using XCT two-dimensional and three-dimensional (3-D) analysis. Features of the damage were correlated with physical processes of damage initiation and growth. The study of this sample is the first known NDE of ballistic damage in this type of lightweight Mg alloy material by XCT or any other NDE method. XCT scans and analyses of damage in the sample will be shown and discussed. This will include virtual 3-D solid visualizations and some quantitative analysis of damage features.

15. SUBJECT TERMS
ballistic damage, Mg, computed tomography, XCT, quantitative

16. SECURITY CLASSIFICATION OF:			17. LIMITATION OF ABSTRACT	18. NUMBER OF PAGES	19a. NAME OF RESPONSIBLE PERSON
a. REPORT	b. ABSTRACT	c. THIS PAGE			William H. Green
Unclassified	Unclassified	Unclassified	UU	24	19b. TELEPHONE NUMBER (*Include area code*) 410-306-0817

Standard Form 298 (Rev. 8/98)
Prescribed by ANSI Std. Z39.18

Contents

List of Figures

1. Introduction

Magnesium (Mg) is being studied for use in lightweight protection systems. Lightweight materials are typically used in armor panel structures in order to decrease weight without losing ballistic performance. Mg is the lightest structural and engineering metal at a density of 1.74 g/cm^3 that is ~1/5, 2/5, and 2/3 the weight of iron, titanium, and aluminum, respectively.[1,2] Mg alloys are being considered as extremely attractive lightweight materials for a wide range of the U.S. Army's future applications where weight reduction is a critical requirement because of its low density. Furthermore, magnesium has good vibration damping capacity[3] and low acoustic impedance characteristics[4] that could be of additional benefit to vehicle applications. X-ray computed tomography (XCT) is an effective and important non-destructive evaluation (NDE) technique for revealing internal fabrication characteristics and spatial distribution of damage in material specimens. Previous and ongoing work in the area of XCT evaluation includes assessment of ballistically induced damage in individual ceramic targets, ceramic panels, and metal plates. The purposes of XCT evaluation include characterization and understanding of the detectable fabrication structure and/or damage in the complete 3-D space of the specimen or scanned volume, determination of geometric parameters of fabrication and/or damage features for interpretation and useful engineering data, and correlation of physical structure with fabrication methods and damage features and types with the physical processes of damage initiation and growth. In this report, the ballistic damage in a novel Mg alloy sample was completely scanned and extensively evaluated using XCT two-dimensional (2-D) and three-dimensional (3-D) analysis.

2. Description of Specimen and Digital Radiography Results

The specimen was an ~146-mm (5.7-in) × 186-mm (7.3-in) rectangular section from a larger impacted test plate with multiple hits, some of which fully penetrated the plate. The specimen included a single complete penetration and the surrounding area as well as undamaged material farther away. Figure 1 shows two photographs of the rear (exit) side of the specimen. The first photograph (figure 1a) shows the relatively large amount of material around the main through

[1]Emley, E. F. *Principles of Magnesium Technology*; Pergamon Press: Oxford, England, 1966.

[2]Avedesian, M. M.; Baker, H., Eds. *Magnesium and Magnesium Alloys*; ASM International: Materials Park, OH, 1999.

[3]Sugimoto, K.; Niiya, K.; Okamoto, T.; Kishitake, K. Study of Damping Capacity in Magnesium Alloys. *Trans. JIM* **1977**, 18, 277–288.

[4]Martin, L. P.; Orlikowski, D.; Nguyen, H. Fabrication and Characterization of Graded Impedance Impactors for Gas Gun Experiments from Tape Cast Metal Powders. *Mat. Sci. Eng. A* **2006**, 427, 83–91.

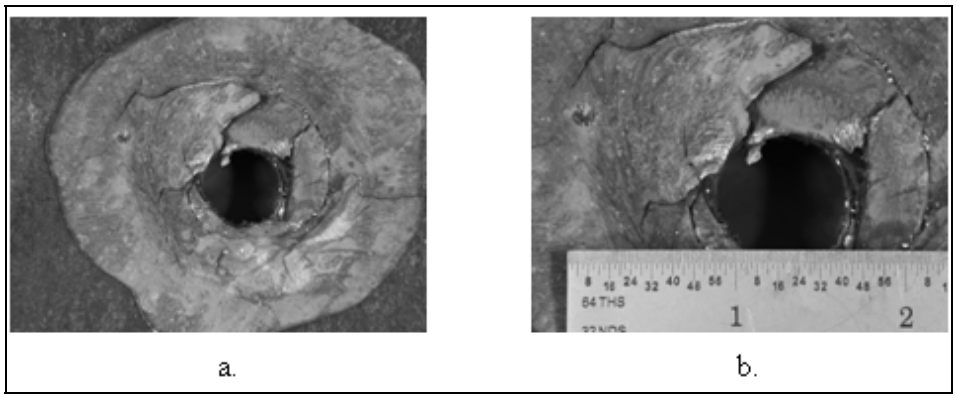

Figure 1. Photographs of rear (exit) side damage in the Mg plate.

hole that was pushed out from the rear of the specimen. The second photograph (figure 1b) includes a ruler to indicate the size of the hole near the rear face, which is ~25 mm across. Digital radiographs (DRs) of the specimen were taken through its thickness and width (edge on) using the 420-keV x-ray tube and linear detector array (LDA) setup in centered rotate-only (RO) mode. The x-ray technique (parameters) of the DRs of the specimen were (400 keV, 2.0 mA) and geometries of source-to-object distance (SOD) = 750.00 mm and source-to-image distance (SID) = 940.00 mm. Figure 2 shows two through thickness DRs (a and b) and one edge on DR (c) of the specimen. The first two DRs have been processed or "windowed" differently to accentuate one or some features over others. In the first, the penetration hole itself is emphasized and shows a darker area to the lower left of the hole due to missing material in the front (impact) side of the specimen. In the second image, the overall damage and the perimeter of the pushed out region of material in the exit side of the specimen is emphasized. It shows the main hole and the region with impact side missing material as all black. In the edge on (side) image of the specimen with the impact side on the left, the main hole is evident, as well as severe damage in the middle and rear regions of the specimen and the missing material that was pushed out of the exit side. This is also the first image that shows some of the nature of the approximately parallel lateral, or "petal-like," damage mode in the middle and towards the rear of the specimen, which is significantly more visible in the cross-sectional XCT images.

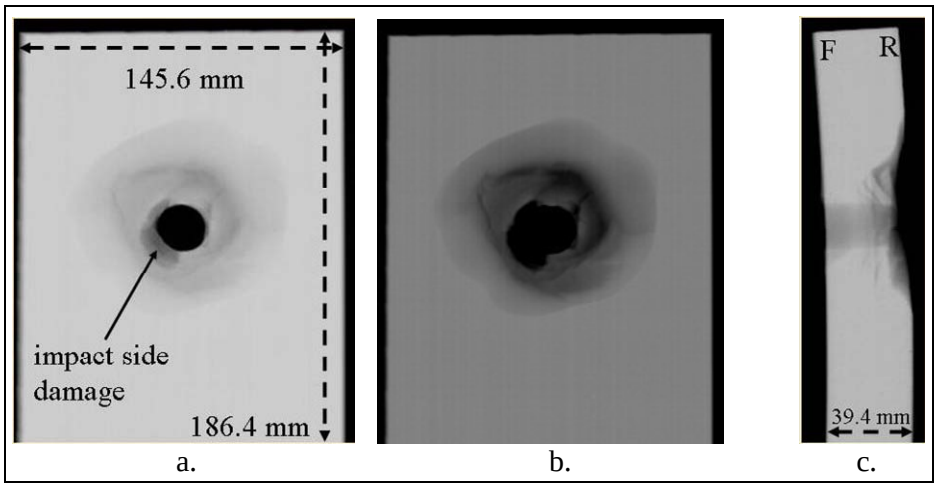

Figure 2. Through thickness (a and b) and edge on (c) digital radiographs of the Mg plate.

3. XCT Scanning Procedures

The specimen stood freely on top of a metal plate to raise it up with its exit side facing the x-ray source. Thus, the specimen faces were perpendicular to the horizontal x-ray (collimated) fan beam resulting in through thickness cross-sectional CT images. The bottom (edge) of the specimen was at a vertical position of about 20 mm and the top was at a position of about 206 mm. The middle of the main penetration hole was at a vertical position of ~116 mm. The entire volume of the specimen between the vertical positions of 65.000 and 173.900 mm was scanned using the 420-keV x-ray tube and LDA set up in offset RO mode. Those two scans were vertically overlapping with a slice thickness and increment of 0.500 and 0.450 mm, respectively, and each slice was reconstructed to a 1024 × 1024 image matrix. The field of reconstruction (FOR) diameter was 195.00 mm. The tube energy and current used were 400 keV and 2.0 mA, respectively, and the focal spot was 0.80 mm. The SOD and SID were 750.00 and 940.00 mm, respectively.

4. Qualitative and Quantitative Evaluation of Specimen

4.1 Computed Tomography Scans

Figure 3 shows a series of CT scans (images) of the specimen, with the first at the vertical position of 116.30 mm (figure 3a), which was within 0.20 mm of the position of the center line of the main penetration hole. The scans in figures 3b–f were taken at vertical positions of 121.25, 126.20, 131.15, 141.05, and 150.95 mm, respectively. The scans in figures 3g–k were

taken at positions of 111.35, 106.40, 101.45, 91.55, and 81.65 mm, respectively. The impact and exit sides of the specimen are at the bottom and top of the images, respectively, and the thickness is 39.4 mm. The missing material towards the front of the specimen adjacent to the main hole is indicated by the shoulder on the right hand side of the cavity wall in figure 3a. A series of approximately parallel lateral, or "petal-like," cracks on both sides of the penetration cavity are evident. The cracks have the appearance of starting in one direction from the sides of the cavity and then turning or bending back from the original direction towards the rear of the specimen. At some depth into the specimen, the lateral damage mode stops and a relatively large amount of material is pushed out of the exit side. The width of the cavity at the very front and rear of the specimen is 31.78 and 90.56 mm, respectively. The narrowest width is 22.27 mm, which is in the middle thickness region. The width of the uppermost cracks towards the rear of the specimen on both the left and right hand side of the penetration cavity is about 1.4 mm. The scans in figures 3b–f are 5.15, 10.10, 15.05, 24.95, and 34.85 mm above the main hole center line, respectively. The parallel lateral cracking damage mode is evident in figures 3b–e, to a lesser extent. These images do not show a high level of cracking oriented approximately in a through thickness direction. The scans in figures 3g–k are 4.75, 9.70, 14.65, 24.55, and 34.45 mm below the center line, respectively. The same lateral damage mode is evident in figures 3g–j, with a similar relative lack of through thickness cracking.

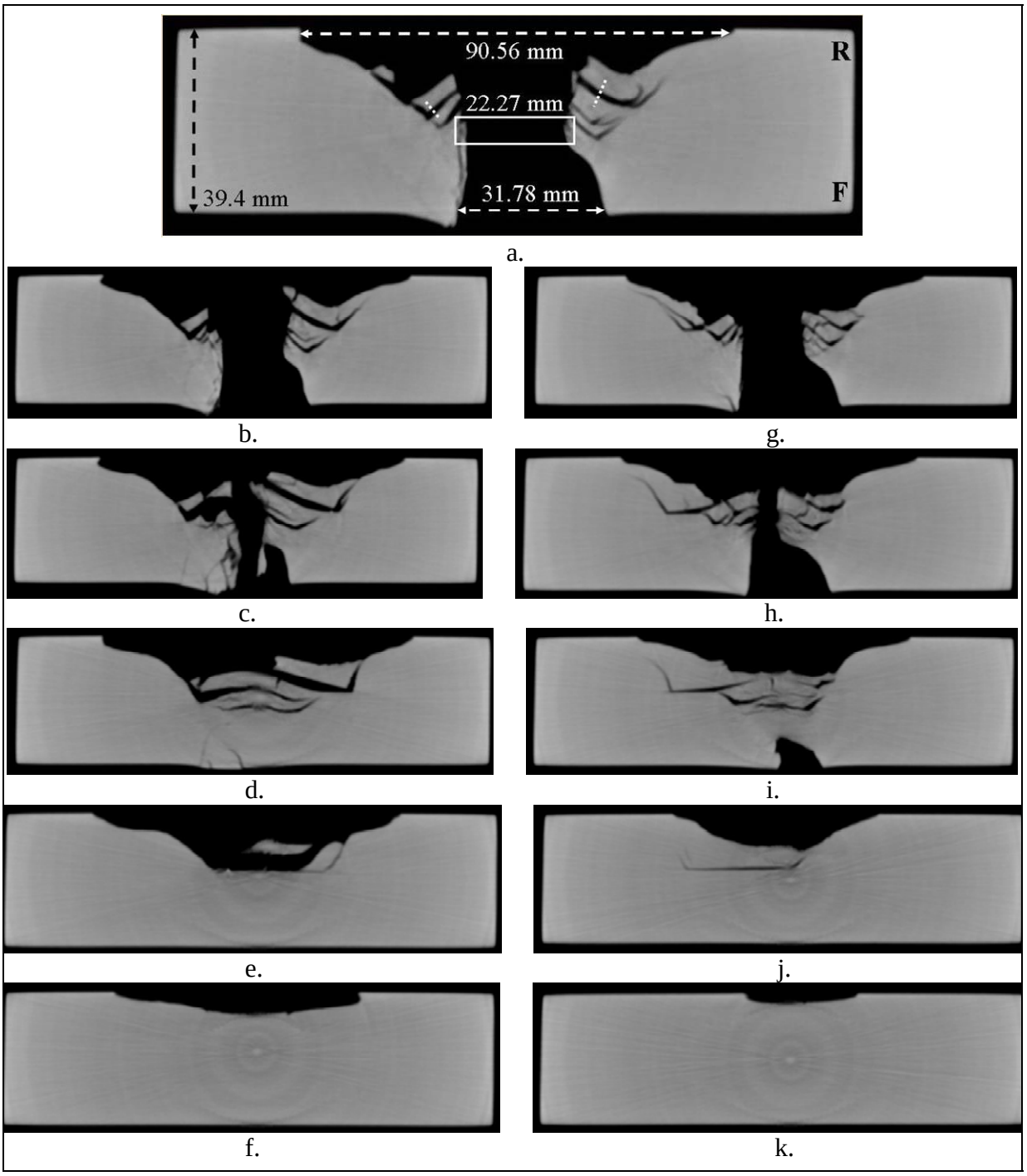

Figure 3. Cross-sectional CT scans (images) of damage in the Mg plate: (a) vertical position of 116.30 mm, (b) 121.25 mm, (c) 126.20 mm, (d) 131.15 mm, (e) 141.05 mm, (f) 150.95 mm, (g) 111.35 mm, (h) 106.40 mm, (i) 101.45 mm, (j) 91.55 mm, and (k) 81.65 mm.

4.2 Three-Dimensional Solid Visualization

The excellent dimensional accuracy and the digital nature of XCT images allow the accurate volume reconstruction of multiple adjacent or overlapping slices. A virtual 3-D solid image is created by electronically stacking the XCT images, which have thickness over their cross-sections (i.e., voxels), one on top of the other from the bottom to the top of the specimen, or scanned height, to generate its virtual volume. Figure 4 shows a set of seven 3-D solid images of the scanned volume with sections virtually removed in figures 4c–g. The method of virtual sectioning, which is essentially only showing a portion of each scan, allows viewing of generated surfaces anywhere in the scanned volume in 3-D space. Figures 4a and b show views of the impact and exit side, respectively, of the entire scanned volume. The very light vertical banding down the middle of the images (top and bottom) is an image artifact from the reconstruction. It is not an indication of a real physical feature in the specimen. The relative shading of lighter and darker gray in the damaged areas is produced by virtual lighting. Physical texture in the surface of the damage in the rear of the specimen is visible in figure 4b. In figure 4c, the impact side of the specimen is at the bottom of the image and the sectioned surface is approximately halfway between the top and the bottom of the main penetration hole. In figure 4d, the sectioned surface is just above the top of the main penetration hole. The relatively lighter surface of the penetration cavity in figures 4c and d is due to the angle of the virtual lighting. In figure 4e, the impact side of the specimen is on the left side of the image and the sectioned surface is approximately halfway between the left and right sides of the main hole. In figure 4f, the sectioned surface is just to the right of the main penetration hole. In figure 4g, two adjacent sectioned surfaces are shown with the impact side of the specimen on the left side of the image. The main penetration hole has been virtually cut in half both horizontally and vertically. All of the sectioned surfaces in figures 4c, e, and g, which are mutually orthogonal, show the parallel lateral cracking damage mode. This is indicative that this damage mode has a significant degree of symmetry about the trajectory of the penetration. Figures 4d and f also show similar damage in the rear side of the specimen.

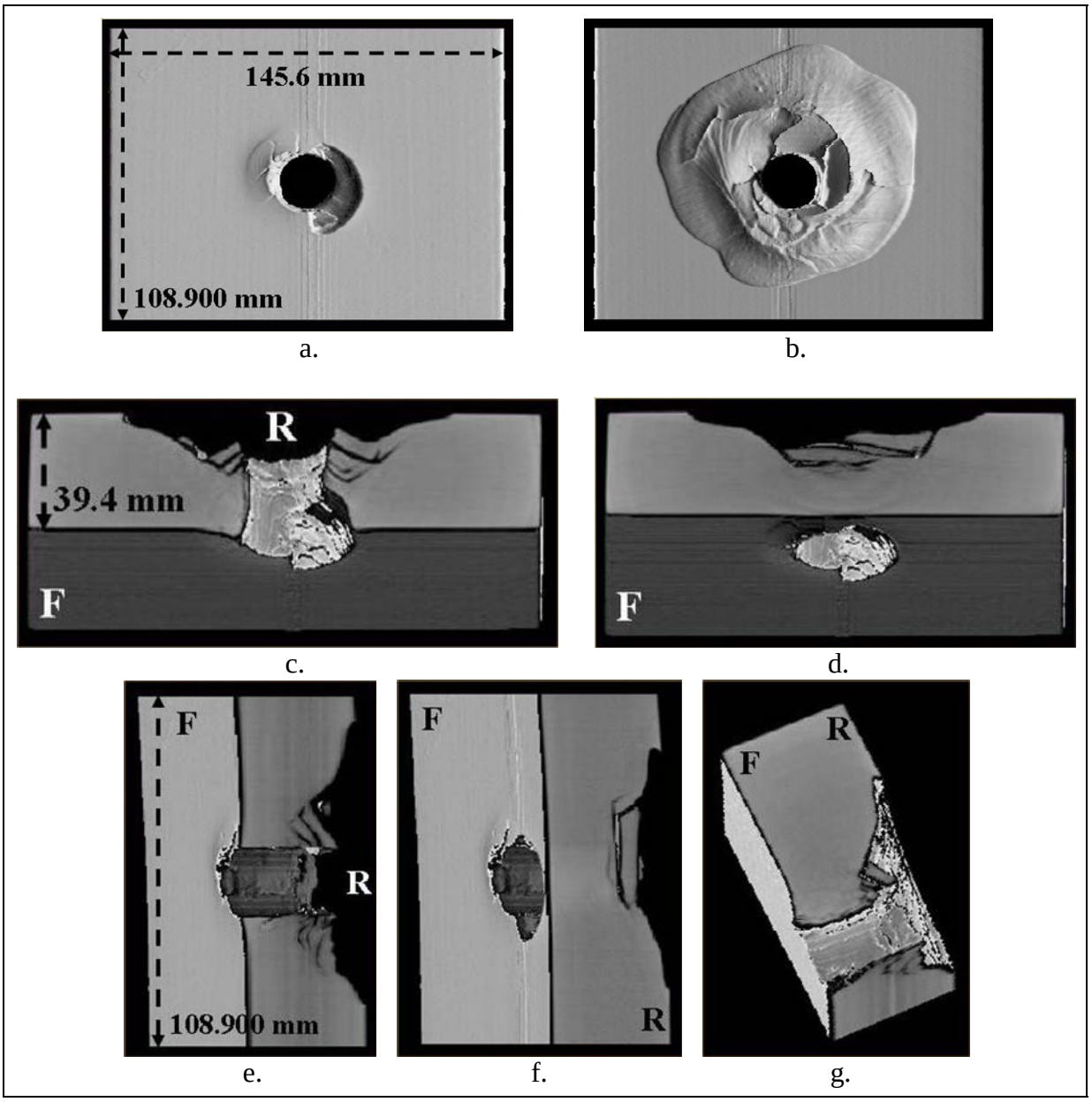

Figure 4. A series of virtual 3-D solid volumes of the damage in the Mg plate: (a) front side, (b) rear side, (c) horizontally sectioned through center of penetration hole, (d) horizontally sectioned just above top of penetration hole, (e) vertically sectioned through center of penetration hole, (f) vertically sectioned just to right of penetration hole, and (g) horizontally and vertically sectioned through center of penetration hole.

4.3 Three-Dimensional Point Cloud Visualization

A 3-D point cloud is a set of points in space that define geometrical characteristics (i.e., shape, size, location) of a specimen or scanned volume and features within it. Location of the points is determined by appropriate (image) segmentation of the volume or feature(s) of interest. Figure 5 is a point cloud of the overall damage in the specimen and its outside surfaces from a top-down view (-z direction) with the impact side at the bottom of the image. This view clearly shows that

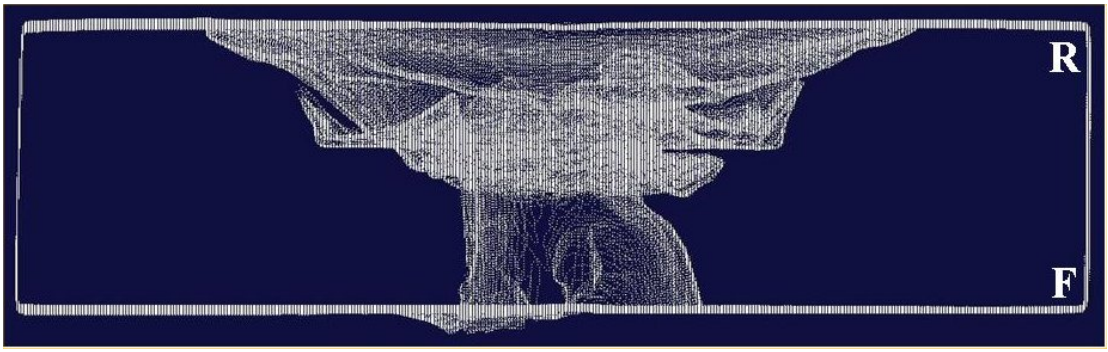

Figure 5. Top-down view of 3-D damage point cloud along with faces and sides of Mg plate (F indicates front and R indicates rear).

there are three distinct regions of different types of damage. The first region of damage towards the front of the specimen with the shoulder on the right is cylindrical and was produced by the initial penetration of the threat. The diameter of the entrance hole without the shoulder included is 21.04 mm with the center at a height of 116.10 mm. The depth and maximum size (parallel to specimen faces) of this region of damage are about 16 and 33 mm, respectively. The middle region of damage, which has clear delineation from the damage towards the front, exhibits multiple parallel lateral cracks with "upturned" ends that go towards the rear of the specimen. The depth of this region to the ends of the cracks closest to the exit face of the specimen is about 16 mm. The maximum distance between the ends (tips) of the upturned cracks is about 68 mm. The last region of damage is the relatively large amount of material that was pushed out of the rear of the specimen, which overlaps with the middle region of damage. The physical morphology of the middle and rear damage regions is closely intertwined, making it difficult to determine a precise boundary between the two regions. The maximum size (parallel to specimen faces) of the rear region of damage is about 100 mm.

Figures 6a and b are isometric views of the damage point cloud only from exit side and impact side perspectives, respectively, with the boundaries of the scanned volume shown in wireframe mode for reference. The face of the specimen that is away from the view perspective is gridded for ease of interpretation. Figures 6c and d are isometric views of the damage point cloud with the front region of damage removed to provide an unobstructed view of the other damage. Figure 7 is a top down view of the point cloud of the rear region of damage with some overlap into the middle damage. Figure 8 is an approximate top-down view of the point cloud of the middle region of damage with a small portion of the rear damage to better show the orientation of the lateral cracks relative to the shallow cone of material pushed out the rear of the specimen. The point cloud is tilted backward a few degrees from a top down view in order to separate the upturned ends of the cracks from the surrounding damage as much as possible. Figure 9 is a top-down view of the point cloud of the front region of damage, with some points on the front surface of the specimen to the left and right of the entrance hole. The surface around the entrance hole on the left side is physically raised on the specimen.

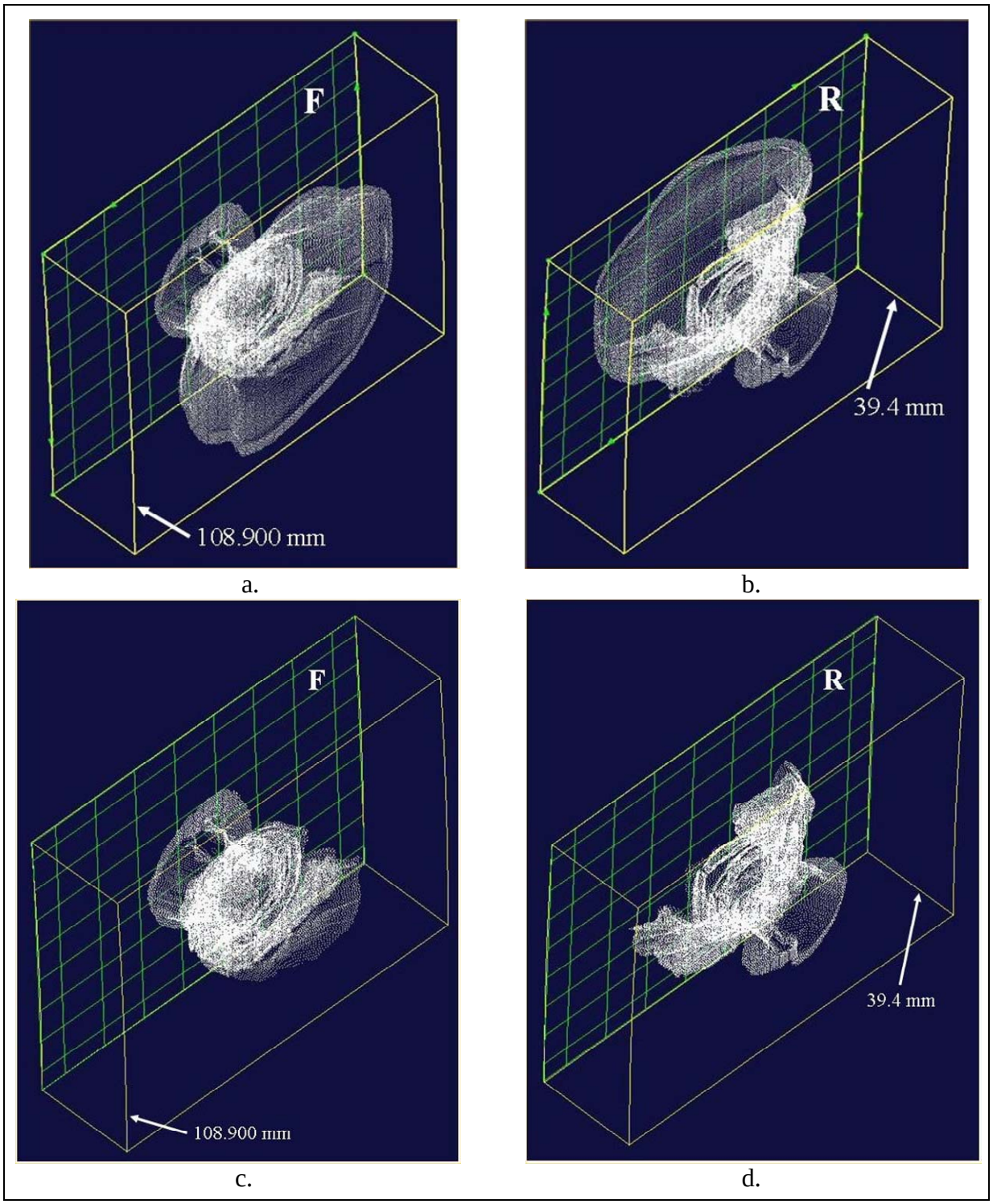

Figure 6. Isometric views of 3-D damage point cloud only with physical boundaries of scanned volume shown as wireframe and face away from the view gridded (F indicates front and R indicates rear): (a) rear view, (b) front view, (c) rear view with rear damage removed, and (d) front view with rear damage removed.

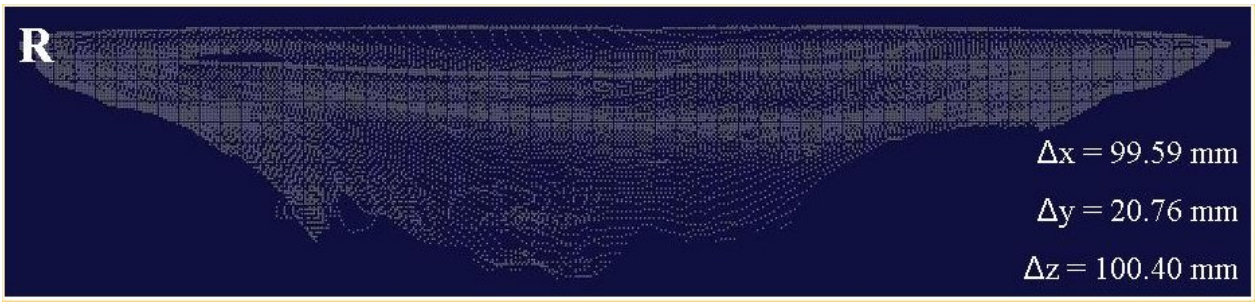

Figure 7. Top-down view of rear section (thickness) of damage point cloud only (R indicates rear side).

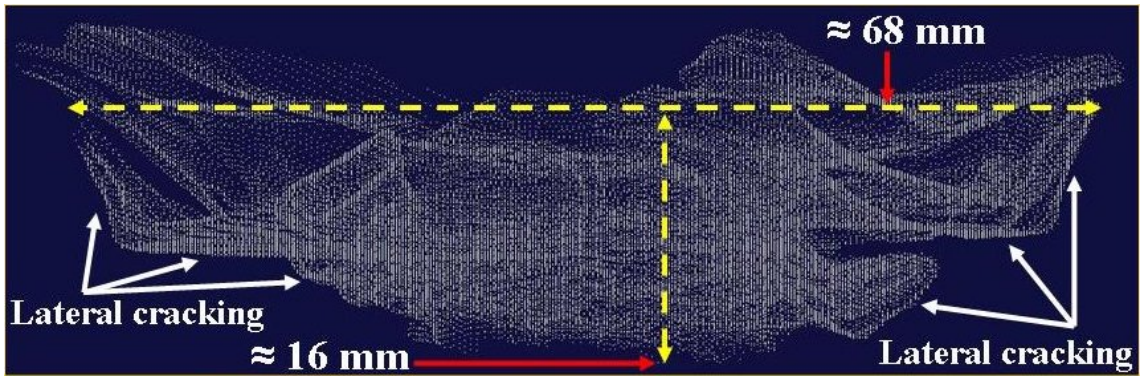

Figure 8. Top-down view of middle section (thickness) of damage point cloud only. The front side of plate is below the bottom of the image.

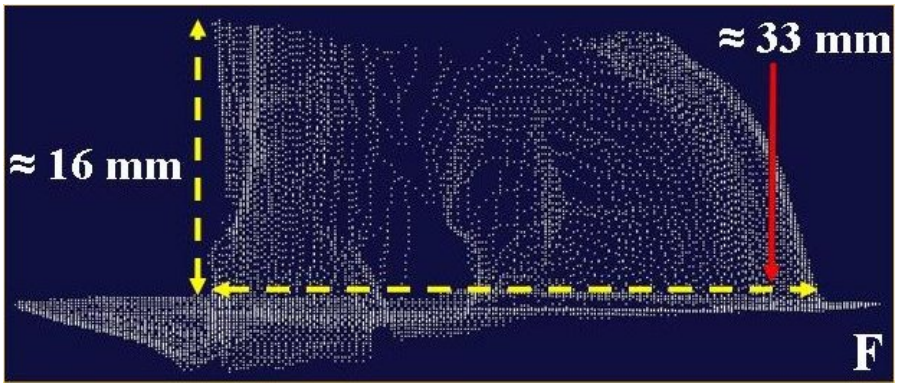

Figure 9. Top-down view of front section (thickness) of damage point cloud only (F indicates front side).

4.4 Quantitative Damage Evaluation and Discussion

Image segmentation can also be used to produce binary (black and white) images in which a gray level threshold is applied to separate a feature or features of interest from the material around it. The gray level width of the segmented images is set to two in order to replace each pixel gray level in the original images with a new minimum or maximum gray level (e.g., 0 or 255 for an 8-bit binary image). The pixel data of binary images can be statistically evaluated to determine the level or severity of features, such as the amount of physically detectable penetration damage. This process was done for the XCT scans starting at the bottom of the penetration cavity, including the material pushed out the rear side. The number of pixels in a damaged state in every other scan (slice) ending at the top of the cavity was determined. The matrix size and area of each scan was (1024 × 1024) and (19.50 × 19.50 cm), respectively, resulting in an area per unit pixel of 0.036 mm^2.

One approach to representing the damage data is to plot the percent damage relative to the cross-sectional area of the specimen against the vertical distance above and below the center line of the penetration cavity. This does show the trend in the overall damage from the bottom to the top of the cavity, as seen in figure 10a. Individual segmented binary XCT scans are overlaid on the plot to show the damage at specific locations. However, in this case the amount of damage is not in terms of an absolute quantity since the cross-sectional area depends in part on the width of the specimen as cut from the larger test plate. A more informative representation of the data is shown in figure 10b in which the pixel area, 0.036 mm^2 from an areal pixel density of 2758 cm^{-2}, was used to convert number of pixels in a damaged state to total damaged area and plot it versus the distance from the center line. Again, individual segmented binary XCT scans are overlaid on the plot to show the damage at specific locations. The most interesting feature of this plot is the shoulder on the right about 20 mm above the center line. The two binary images shown in this vicinity appear to indicate that less material remained on the left side of the penetration cavity. Figure 10c shows the damaged area plot as well as minimum possible damage from complete penetration and normalized damaged area plots.

The minimum damage plot (triangles) is based on the amount of damage that would be present due to a uniform penetration hole through the thickness of the specimen with a diameter equal to the diameter of the base of the threat. Therefore, the minimum damage is 0 if the distance above or below the center line is one threat radius or greater. The normalized damaged area plot (squares) is simply the damaged area plot (black diamonds) divided by the minimum damage plot. It shows that the damaged area produced by the penetration at the center line is approximately 5× greater than the damage that would exist from a minimum complete penetration hole.

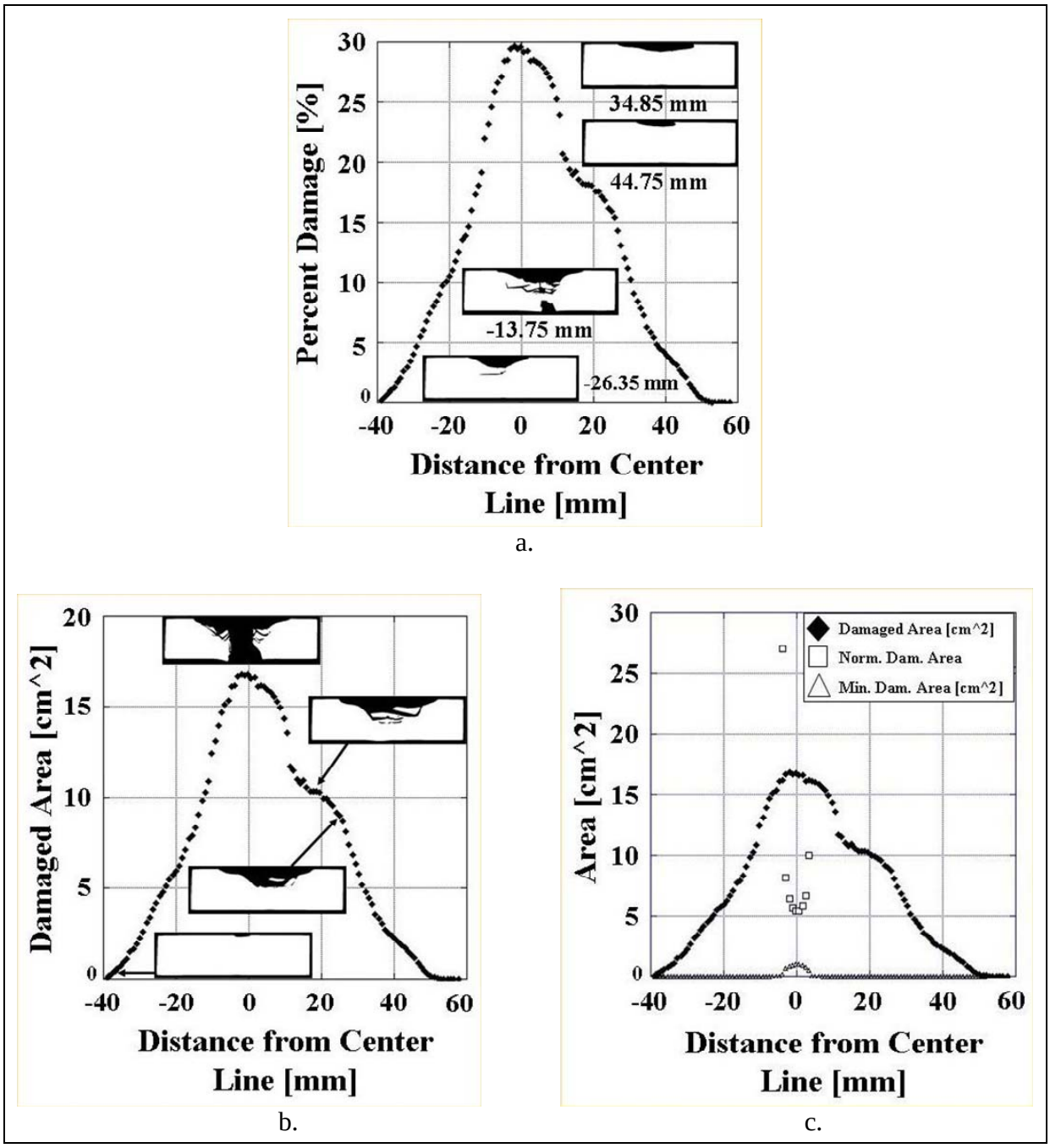

Figure 10. Plots of damage vs. vertical distance from center line of penetration cavity (positive indicates above and negative indicates below center line): (a) percent damaged area perpendicular to faces, (b) damaged area perpendicular to faces, and (c) damaged area, minimum damage area, and normalized damaged area on same plot for comparison.

Multiplanar reconstruction (MPR) visualization, also a form of volume reconstruction, used the same set of XCT images as the 3-D solid visualization and was applied to generate individual virtual vertical slices of the specimen from its impact face to its exit face, which were also segmented to binary images. The areal pixel density of views in a MPR image, of which there

are four (top, side, front, and oblique), is determined differently than XCT images, since each view is not a single reconstructed image to a set matrix size like a CT image. In this case, the physical area of the specimen and the average number of pixels in that area in the vertical slices (front views) of the MPR images was (14.56 × 10.89 cm) and 109,114 pixels, respectively. This resulted in an areal pixel density of 688 cm^{-2} and inversely a pixel area of 0.145 mm^2.

Figure 11a is a plot of the percent damaged area parallel to the faces of the specimen versus depth from its impact face. Individual segmented binary vertical slices are overlaid on the plot to show the damage at specific locations. Figure 11b is a plot of the damaged area parallel to the faces of the specimen versus depth from its impact face. Again, individual segmented binary vertical slices are overlaid on the plot to show the damage at specific locations. The plot has two local maxima and three local minima. This behavior of local peaks and valleys is due to the parallel lateral cracking damage mode in the middle of the specimen. The local spatial periodicity of the minima-to-minima (two) and maxima-to-maxima (one) segments of the damage is about 5 mm. The plot also shows that the area of the penetration hole necks down to a minimum at a depth of about 14 mm and a steep rise after a depth of about 26 mm, which is indicative of the large amount of material pushed out the back of the specimen. Figure 11c shows the damaged area plot as well as normalized minimum and normalized damaged area plots. Again, the normalized minimum plot (triangles) is based on the amount of damage that would be present due to a uniform penetration hole through the thickness of the specimen with a diameter equal to the diameter of the base of the threat. In this case, the minimum possible damage area as a function of depth is a constant, so this plot is normalized to one. The normalized damaged area plot (squares) is the damaged area plot (black diamonds) divided by the constant minimum damage area. In this way, the normalized damaged area plot gives a factor difference between the actual damaged area and the minimum possible damage with complete penetration (factor = 1). For example, at a depth of about 14 mm the damaged area is about nine times greater than the minimum possible damage area for a uniform through thickness hole. Similarly, at the two depths of the local maxima, about 18 and 22.5 mm, the damaged area is about 20 and 37× greater than the minimum, respectively. The through-thickness damaged area is at least approximately one order of magnitude or greater than the minimum possible damage area throughout the penetration cavity.

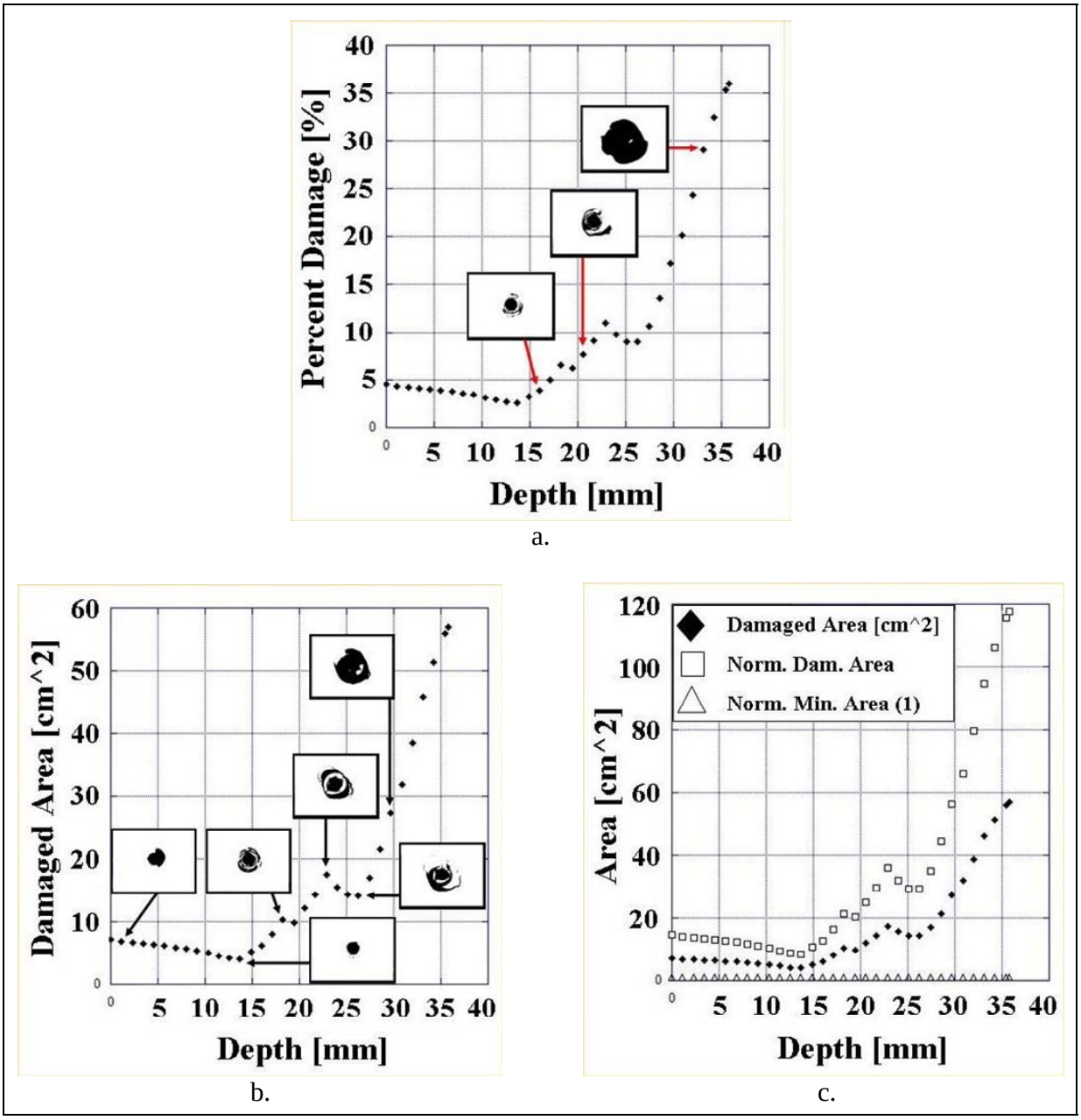

Figure 11. Plots of damage vs. depth (distance from front face): (a) percent damaged area parallel to faces, (b) damaged area parallel to faces, and (c) damaged area, normalized minimum area, and normalized damaged area on same plot for comparison.

5. Conclusions

Ballistic damage in a sectioned specimen from a larger novel Mg plate was scanned and extensively characterized using XCT 2-D cross-sectional (planar) and 3-D volumetric analysis. Damage features including near parallel lateral cracking with “upturned” ends away from the penetration cavity, narrowing and widening cylindrical section of the penetration cavity, asymmetric missing material on one side of the impact face, relatively large area removal of material on the exit side, and three zones of different types of damage and features were captured and discussed. Successive application of XCT 2-D evaluation, volumetric solid visualization and analysis, and volumetric point cloud visualization and analysis provided extensive and important qualitative and quantitative data about damage features. The amount of detectable damage both as a function of the distance from the impact side (depth) and the vertical distance from the center line of the penetration cavity was determined and plotted. The damaged area data was also normalized relative to an appropriate area and plotted. Both sets of data (depth and vertical distance) exhibited features in their plots, including an asymmetric shoulder and local minima and maxima, quantitatively reflecting particular characteristics of the damage. Characteristics of captured damage features provided better understanding of the physical processes of damage initiation and growth. Future work is planned to further analyze the damage features and plot data in conjunction with microstructural observations and evaluation using relevant approaches and specimens from the Mg plate.

NO. OF
COPIES ORGANIZATION

1 (PDF only) DEFENSE TECHNICAL INFORMATION CTR
DTIC OCA
8725 JOHN J KINGMAN RD
STE 0944
FORT BELVOIR VA 22060-6218

1 DIRECTOR
US ARMY RESEARCH LAB
IMNE ALC HRR
2800 POWDER MILL RD
ADELPHI MD 20783-1197

1 DIRECTOR
US ARMY RESEARCH LAB
RDRL CIM L
2800 POWDER MILL RD
ADELPHI MD 20783-1197

1 DIRECTOR
US ARMY RESEARCH LAB
RDRL CIM P
2800 POWDER MILL RD
ADELPHI MD 20783-1197

1 DIRECTOR
US ARMY RESEARCH LAB
RDRL D
2800 POWDER MILL RD
ADELPHI MD 20783-1197

ABERDEEN PROVING GROUND

1 DIR USARL
RDRL CIM G (BLDG 4600)

NO. OF
COPIES ORGANIZATION

ABERDEEN PROVING GROUND

9 DIR USARL
RDRL WMM D
E CHIN
K CHO
W GREEN (4 CPS)
R SQUILLACIOTI
RDRL WMM E
H MILLER
RDRL WMM F
J MONTGOMERY

INTENTIONALLY LEFT BLANK.